INSTITUTE OF PHYSICS PUBLISHING PLASMA SOURCES SCIENCE AND TECHNOLOGY
Plasma Sources Sci. Technol. **14** (2005) 314–320 doi:10.1088/0963-0252/14/2/013

# Comparison of an atmospheric pressure, radio-frequency discharge operating in the $\alpha$ and $\gamma$ modes

**X Yang[1], M Moravej[1], G R Nowling[1], S E Babayan[2], J Panelon[2], J P Chang[1] and R F Hicks[1]**

[1] Chemical Engineering Department, University of California, Los Angeles, CA 90095, USA
[2] Surfx Technologies LLC, 3617 Hayden Ave., Culver City, CA 90232, USA

E-mail: rhicks@ucla.edu

Received 23 July 2004
Published 22 March 2005
Online at stacks.iop.org/PSST/14/314

**Abstract**
The $\alpha$ and $\gamma$ modes of an atmospheric pressure, radio-frequency plasma have been investigated. The plasma source consisted of two parallel electrodes that were fed with helium and 0.4 vol% nitrogen. The transition from $\alpha$ to $\gamma$ was accompanied by a 40% drop in voltage, a 12% decrease in current and a surge in power density from 25 to 2083 W cm$^{-3}$. Optical emission confirmed that sheath breakdown occurred at the transition point. The maximum light intensity shifted from a position 0.25 mm above the electrodes to right against the metal surfaces. The average density of ground-state nitrogen atoms produced in the atmospheric plasma was determined from the temporal decay of $N_2(B)$ emission in the afterglow. It was found that 5.2% and 15.2% of the $N_2$ fed were dissociated into atoms when the plasma was operated in the $\alpha$ and $\gamma$ modes, respectively. The lower efficiency of the $\gamma$ discharge may be attributed to the non-uniform distribution of the discharge between the electrodes.

(Some figures in this article are in colour only in the electronic version)

## 1. Introduction

Plasma technologies play a vital role in materials processing for the microelectronics, automotive, aerospace and bio-medical industries. Chemically reactive plasma discharges are widely used for etching, thin film deposition, surface activation and bio-sterilization [1, 2]. Recently, there has been increased interest in using atmospheric pressure plasmas for materials processing [3–15]. These plasmas do not require vacuum systems and are suitable for continuous in-line processing. Thermal atmospheric plasmas, i.e. torches, may be used when the substrates are not thermally sensitive, or when the contact time can be kept very short [4]. Low-temperature atmospheric plasmas include coronas [10], dielectric barrier discharges [11, 12], microhollow cathode discharges [13], the one-atmosphere-uniform-glow-discharge plasma (OAUGDP) [14] and surface-wave discharges [15]. Coronas have been well studied since they were introduced several decades ago. However, the other designs were developed more recently and are increasingly used for materials processing.

We have shown that a stable, capacitive discharge may be produced at atmospheric pressure by feeding helium or argon between two metal electrodes driven with radio-frequency (RF) power at 13.56 MHz [3, 16–26]. This plasma operates at temperatures below 100°C and is homogenous in space and time. A high density of reactive species is generated in the source, which is suitable for the downstream processing of substrates, regardless of their size, thickness or shape [17, 21, 24]. So far this plasma source has been used for plasma-enhanced chemical vapour deposition of silicon oxide, silicon nitride and amorphous hydrogenated silicon [20, 22, 25]. In addition, the atmospheric plasma has been applied to the etching of kapton, silicon dioxide, tantalum and uranium oxide [16, 18, 26].

RF capacitive discharges at moderate pressure (10–200 Torr) have been studied for many years [28–33]. Raizer *et al* [29–32] have shown that these plasmas may

exist in two operating modes, $\alpha$ and $\gamma$, depending on the dominant ionization process. In the $\alpha$ mode, the plasma is sustained by bulk ionization, while in the $\gamma$ mode, it is sustained by secondary electron emission from the electrode surface. Sheath breakdown causes the transition from the bulk to the surface, i.e. the $\gamma$ discharge occurs when the oscillation amplitude of the plasma boundary exceeds half the total thickness of the $\alpha$ sheath.

An atmospheric pressure, capacitive discharge plasma, fed with helium gas, has been examined by Park *et al* [19]. They found that their parallel-plate source could be operated in the $\alpha$ mode up to a current density of 38 mA cm$^{-2}$, and thereafter it converted to a filamentary arc. Recently, Shi *et al* [8] reported that a new operating regime may be produced in atmospheric pressure helium plasmas. They denoted this regime the 'recovery mode', and showed that it consumed much greater quantities of RF power. Their electrode design consisted of a powered metal pin held a few millimetres above a grounded metal plate. The transition to the 'recovery' mode was most likely due to sheath breakdown as observed in capacitive discharges operated at moderate pressures.

In this paper, we describe the properties of the $\alpha$ and $\gamma$ operating modes of an atmospheric pressure, RF plasma, fed with helium and nitrogen. This system has been studied with current, voltage and power measurements and optical emission spectroscopy. Furthermore, we have determined the concentration of ground-state nitrogen atoms produced in the plasma. Somewhat surprisingly, the reactive species density is only three times higher in the $\gamma$ mode compared to the $\alpha$ mode.

## 2. Experimental methods

A schematic of the atmospheric pressure plasma used in these experiments is shown in figure 1. It consisted of two parallel electrodes made of aluminium and separated by a gap of 1.6 mm across. The upper electrode was 7.6 × 7.6 mm$^2$, and was connected to an RF power supply (13.56 MHz). It was

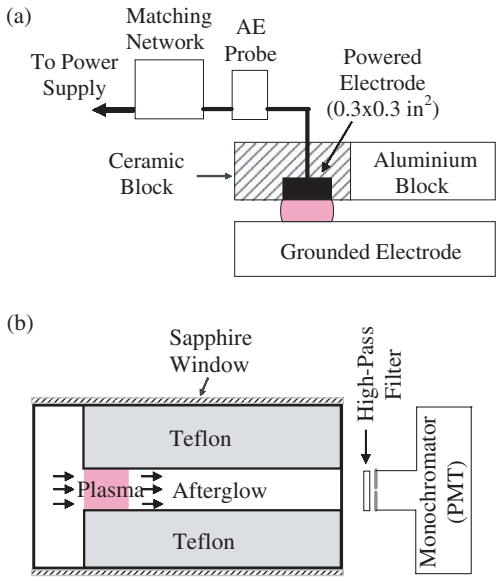


**Figure 1.** Schematic of the experimental apparatus: (*a*) side view, (*b*) top view.

embedded in a ceramic block of dimensions 10.2 × 10.2 cm$^2$. An aluminium block, 10.2 × 10.2 cm$^2$, was placed downstream of this electrode. The lower electrode, 10.2 cm wide and 20.4 cm long, was grounded and cooled with chilled water. The upper electrode was positioned above the centre of the lower electrode. These parts were assembled together to provide a uniform duct 1.6 mm in height throughout the length of the device. Teflon spacers were placed in the duct to force the gas to flow past the upper electrode. The matching network was an 'L' configuration with an inductor of 2.1 $\mu$H. The load and tune capacitors were variable in the range of 7 pF to 1000 pF and 12 pF to 500 pF, respectively. A tuned impedance probe (Advanced Energy RFZ 60) was inserted between the matching network and the plasma source, eliminating any cable connections, which might add inductance to the system. The plasma voltage as a function of current was determined with the advanced energy probe, which also yielded information on the impedance, reactance, resistance and phase angle.

The plasma was operated at a total flow rate of 12.8 litre min$^{-1}$, 748 Torr of helium and 3.4 Torr of nitrogen. The flow rate produced a linear velocity of 18 m s$^{-1}$. The corresponding Reynolds number was 250, which was well within the laminar-flow regime. Helium of ultrahigh purity (99.999%) was purified by a SAES Getter to <10 parts per billion (ppb) prior to induction into the plasma source. Nitrogen was of ultrahigh purity (99.999%). The neutral gas temperature was determined by calculating the rotational temperature of the (3,0) band of the $N_2$ first positive emission spectrum [34]. The gas temperature obtained in this way agreed with the temperature measured from an ungrounded thermocouple to within 20 K.

The transient decay of the emission from $N_2(B)$ and excited nitrogen atoms, after turning off the plasma, was measured with a photo-multiplier tube (PMT) (Hamamatsu, R928P) attached to the monochromator. The PMT was positioned at the outlet of the discharge so that the plasma emission could be observed parallel to the flow direction (see figure 1(*b*)). The RF power was delivered in 50 ms pulses with a 20% duty cycle. A power sampler monitored the voltage signal and triggered the oscilloscope (Tektronix TDS 224) to record the data.

The atomic nitrogen concentration was calculated from the temporal intensities of the $N_2(B, v)$ signal using the following relation derived in a previous paper [21]:

$$[\mathrm{N}(t)] = \frac{-\mathrm{d}\ln I_{\mathrm{N}_2(B,v')}(t)/\mathrm{d}t}{4k_{\mathrm{re}}(\mathrm{He})[\mathrm{He}]}, \qquad (1)$$

where $k_{\mathrm{re}}$ is the rate constant for the three-body recombination of ground-state N atoms:

$$\mathrm{N} + \mathrm{N} + \mathrm{He} \longrightarrow \mathrm{N}_2(B) + \mathrm{He}. \qquad (\mathrm{R1})$$

This is the primary consumption reaction of nitrogen atoms in the plasma afterglow. The value of $k_{\mathrm{re}}$ is 2.2 × 10$^{-33}$ cm$^6$ s$^{-1}$ [21]. This method of obtaining the N-atom density from optical emission spectroscopy of the $N_2(B)$ state is well established [35–37]. Furthermore, in our earlier work, we verified the results obtained from equation (1) by comparison with nitric oxide titration of the N atoms [21].

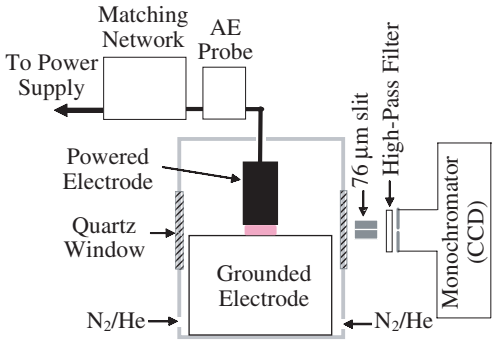


**Figure 2.** Schematic of the plasma source used for the photographs and emission profiles.

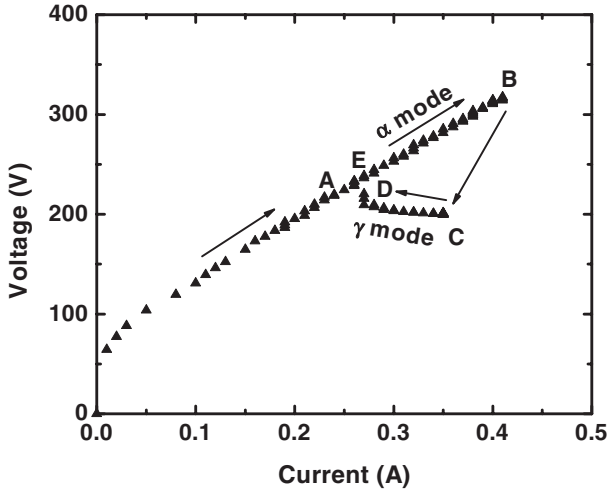


**Figure 3.** *I–V* curve for the atmospheric pressure helium and nitrogen plasma with the arrow showing the sequence of operating conditions employed.

To take photographs of the discharge, an alternative plasma source shown in figure 2 was used. The source consisted of two aluminium rods with faces parallel to each other and separated by a 3.0 mm gap. The powered electrode was 9.0 mm in diameter, while the grounded electrode was 40 mm in diameter. The plasma was housed in a cylindrical plastic container with quartz windows. To determine the spatial profiles of the light emission between the two electrodes, a slit 76 $\mu$m wide was cut through a 1.6 cm thick piece of aluminium. This slit was placed between the source and the detector, and provided a resolution of 150 $\mu$m. The emitted light passed through a 550 nm high-pass filter and into a monochromator (Instruments, S.A., Triax 320). The spectrometer was equipped with a 1200 groove mm$^{-1}$ grating and a liquid nitrogen cooled CCD detector (Instruments, S.A., CCD-3000).

## 3. Results

### *3.1. Current–voltage characteristics*

In figure 3 we show the current–voltage ($I$–$V$) curve for the helium and nitrogen plasma. A pink glow discharge is struck at a voltage and current of 229 V and 0.26 A, respectively (point A in the figure). The discharge voltage increases linearly

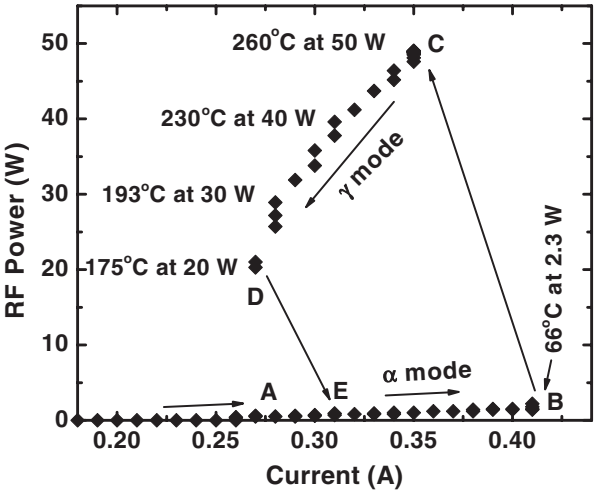


**Figure 4.** The dependence of the absorbed power and gas temperature on the discharge current with the arrow showing the sequence of operating conditions employed.

with the current with increasing input power, as shown from points A to B. This is the abnormal glow operating regime that has been observed in other studies of the atmospheric plasma [8, 9, 19, 38, 39]. As will become apparent below, the abnormal glow is an $\alpha$-mode discharge.

Upon increasing the power further an abrupt transition occurs from points B to C. Here, the voltage drops from 317 to 200 V, the current decreases from 0.41 to 0.35 A and the power surges from 2.3 to 50 W. At the same time, the phase angle changes from 88.9° to 45.7°, indicating that the discharge has become more resistive. Decreasing the power results in a drop in current at an approximately constant voltage from C to D. A second transition occurs at D to E, where the plasma reverts to the abnormal glow. If the input power is raised again, the $I$–$V$ trend will be retraced from points E to B to C to D and back again. The large power surge observed at C is due to the breakdown of the $\alpha$-mode sheath and the formation of the $\gamma$-mode discharge. It should be noted that the matching network setting was fixed during the mode transition.

### *3.2. Dissipated plasma power and neutral gas temperature*

In figure 4 we show the dependence of the dissipated power on the discharge current. The neutral gas temperatures at different plasma powers are also presented. The maximum power absorbed by the plasma in the $\alpha$ mode is only 2.3 W, corresponding to a power density of 25 W cm$^{-3}$. An abrupt increase of plasma power from 2.3 to 50 W occurs as the discharge transforms from the $\alpha$ to the $\gamma$ mode at point B to C. The corresponding power density is 2083 W cm$^{-3}$ at C, which is an 85-fold increase. The power density is calculated while taking into account changes in the plasma volume. Upon decreasing the input power down to D, the absorbed RF energy decreases linearly with the current from 50 to 20 W. Finally, from D to E, the plasma returns to the $\alpha$ mode and the dissipated power drops from 19 to 0.9 W.

The neutral temperature follows a similar trend with the plasma power. It jumps from 66°C to 260°C at the $\alpha$–$\gamma$ transition, and decreases down to 175°C at point D. Then, the gas temperature drops abruptly from 175°C to 55°C as the

plasma returns to the abnormal glow regime at E. A 5–10 min operation of the plasma at 50 W does not damage the surface of the electrodes. Note, however, that severe damage occurs if the plasma is allowed to transform into an arc [19].

Shi *et al* [8] observed analogous current, voltage and power trends as those reported here, including the high-power operating regime between points C and D in figures 3 and 4. It should be noted that the $\alpha$–$\gamma$ transition from B to C may be accompanied by either a decrease (cf figure 3) or an increase in the current. We have found that this difference depends solely on the design of the matching network.

### *3.3. Photographs and emission intensity profiles between the electrodes*

A photograph of the plasma at point B in the $I$–$V$ curve is shown in figure 5, where the white line indicates the boundaries of the electrodes. One sees that a fairly uniform pink glow fills the gap between the two electrodes. A layered structure is observed in the direction perpendicular to the electrodes. Adjacent to the metal surfaces and in the centre of the gap the plasma is relatively dim, whereas a bright region exists 0.25 mm away from the boundaries.

Figure 6 shows the spatial profile of the helium I emission at 706.5 nm. It can be seen that the emission intensity is symmetric, reaching a maximum 0.25 mm away from the electrodes, and a minimum in the centre of the gap. The centre dark region is about 1.4 mm wide. The emission intensity decreases to about one-third of the maximum at the surfaces of the electrodes. The layered structure illustrated in figures 5 and 6 is characteristic of an $\alpha$ discharge in which the plasma is sustained by bulk ionization of the gas.

In figure 7 we show a photograph of the discharge at point C in the $I$–$V$ curve. Here, the glow takes on a barbell shape. Bright circular discs 4.5 mm in diameter by 0.5 mm thick are centred at the electrode surfaces. These discs are connected by a dimmer column of light 1.7 mm in diameter. Changing the input power only affects the brightness of the discharge but not its size or shape. The intense emission centred at the electrodes is consistent with a $\gamma$-mode discharge in which ionization is dominated by secondary electron emission from the metal surfaces.

The intensity of the $\gamma$ discharge is symmetric across the gap, as illustrated in figure 8. This plasma exhibits a maximum emission intensity at the boundaries. The emission falls to a very low value about 0.4 mm away from the metal surfaces. A comparison of figure 8 with figure 6 reveals that the maximum intensity in the $\gamma$ discharge is 220 times greater than that in the $\alpha$ discharge.

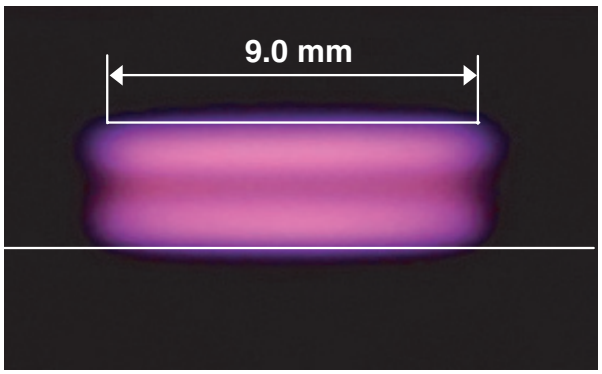


**Figure 5.** Photograph of the atmospheric plasma operated in the $\alpha$ mode.

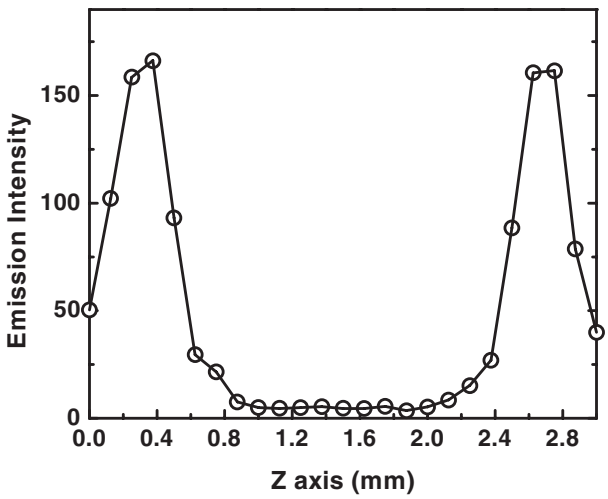


**Figure 6.** Spatial profile of the emission intensity between the electrodes for the $\alpha$ discharge.

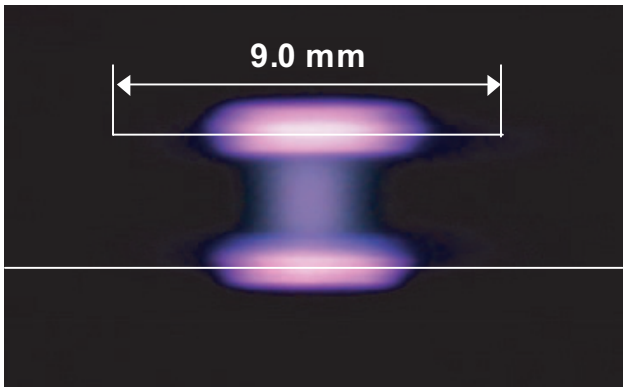


**Figure 7.** Photograph of the atmospheric plasma operated in the $\gamma$ mode.

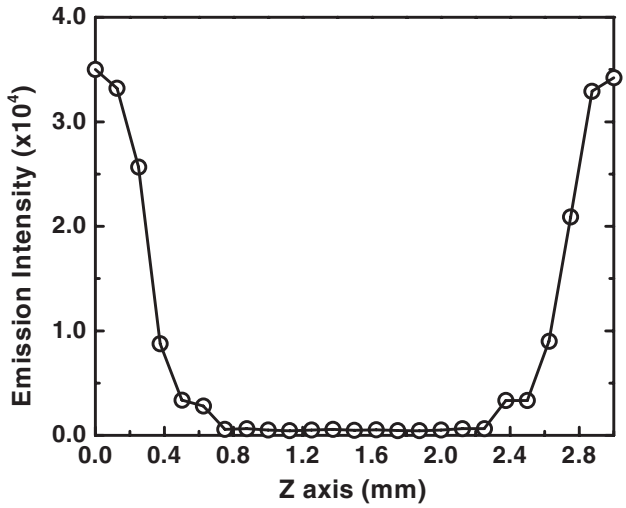


**Figure 8.** Spatial profile of the emission intensity between the electrodes for the $\gamma$ discharge.

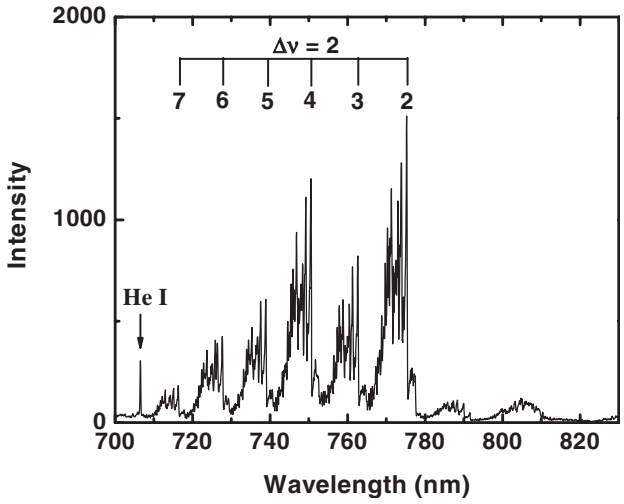


**Figure 9.** Optical emission spectrum of the atmospheric plasma operated in the $\alpha$ mode.

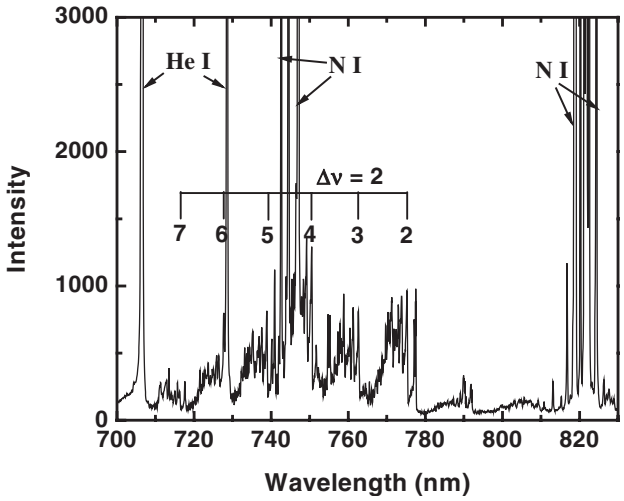


**Figure 10.** Optical emission spectrum of the atmospheric plasma operated in the $\gamma$ mode.

In summary, the photographs and spatial emission profiles observed here for the atmospheric pressure plasma have the same characteristics as the $\alpha$- and $\gamma$-mode discharges investigated in the past at low and moderate pressures [29]. This further confirms the existence of the two ionization mechanisms for the atmospheric pressure helium and nitrogen plasma.

### *3.4. Optical emission spectra of the $\alpha$- and $\gamma$-mode discharges*

In figure 9 we show the optical emission spectrum of the helium and 0.4 vol% nitrogen plasma operating in the $\alpha$ mode. One sees bands due to the helium I atomic line at 706.5 nm and the $N_2(B\,^3\Pi$ to $A\,^3\Sigma)$ transition for $\Delta\nu = 2$. Other transitions of $N_2(B)$, $\Delta\nu = 1$, 3 and 4, are observed, but are not shown in the figure [23, 40]. Note that the maximum $N_2(B)$ emission intensity at a position 0.25 mm from the electrodes is 1.5 times higher than that at the centre of the gap. Nitrogen atomic lines are not observed in these spectra. Even the seven-line multiplet in the range 818.5–824.2 nm cannot be detected [41].

The emission spectrum of the helium and nitrogen plasma operating in the $\gamma$ mode is presented in figure 10. These data were recorded at a position close to the electrode surface where the intensity is near its maximum. Strong helium atomic lines at 706.5 and 728.5 nm are detected [41]. In addition, one sees strong nitrogen atomic lines at 742.6, 744.5 and 747.0 nm due to transitions from $^4S^o$ ($J = \frac{3}{2}$) to $^4P$ ($J = \frac{1}{2}, \frac{3}{2}, \frac{5}{2}$), and the seven-line multiplet between 818.5 and 824.2 nm due to $^4P^o$ ($J = \frac{1}{2}, \frac{3}{2}, \frac{5}{2}$) to $^4P$ ($J = \frac{1}{2}, \frac{3}{2}, \frac{5}{2}$) [41, 42]. The overall intensity of this spectrum is about five times higher than that at the centre of the gap.

### *3.5. Temporal decay of $N_2(B)$ emission and nitrogen atom density*

In figure 11 we show the temporal decay profiles for the $N_2(B, \nu = 7)$ emission at 653.0 nm for the $\alpha$- and $\gamma$-mode discharges. For the latter case, the transient decay curve of the nitrogen atomic emission at 745.6 nm is plotted as well.

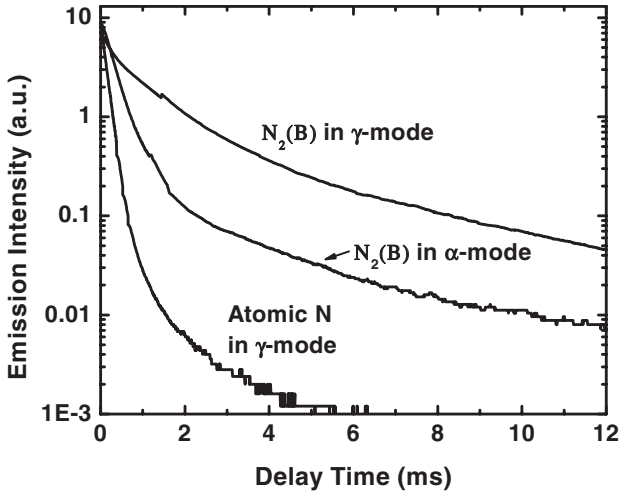


**Figure 11.** Temporal decay profiles of $N_2(B)$ and atomic N emission lines in the plasma afterglow.

It can be seen that the intensity of the nitrogen atomic emission decays extremely fast. Just 1.5 ms after the plasma has been extinguished, the intensity of this line has fallen three orders of magnitude. This is due to the frequent collisions of the excited N atoms with helium at atmospheric pressure. The psuedo-first-order rate constant for the deactivation reaction is approximately $10^7\ s^{-1}$ [43]. Consequently, it is reasonable to assume that all the nitrogen atoms are in the ground state, $N(^4S)$, beyond a delay time of 2.5 ms. Note that at smaller delay times, the $N_2(B)$ emission intensity does not decay at the same rate for the $\alpha$- and $\gamma$-mode discharges. This difference may be attributed to the existence of several pathways for creating $N_2(B)$ in the early afterglow. Nevertheless, beyond 2.5 ms, the two curves are parallel to each other, indicating that the same mechanism is operative, i.e. the three-body recombination of ground-state N atoms into $N_2(B)$ [21].

The inverse of the derivative of the $N_2(B)$ emission intensity, $1/(\mathrm{d}\ln(I_{N_2(B)}(t))/\mathrm{d}t)$, is plotted versus time for the $\alpha$ and $\gamma$ modes in figure 12. The dashed lines represent the 'best fit' to the data from 2.5 to 10 ms. Both lines exhibit a

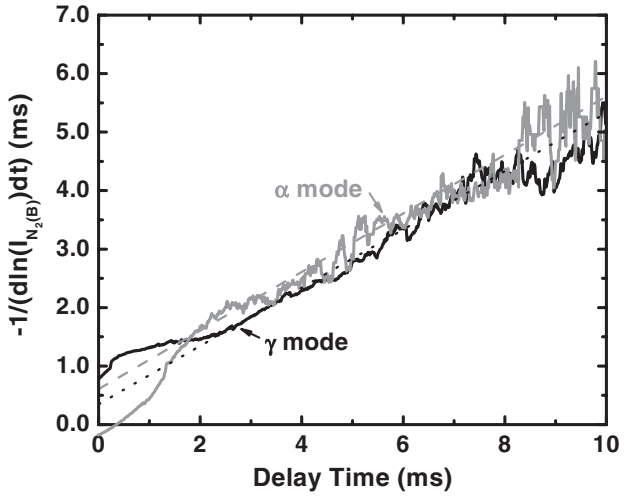


**Figure 12.** The dependence of the inverse derivative of the $N_2(B, v = 7)$ intensity on time after the discharge has been switched off.

slope of $0.49 \pm 0.03$, in good agreement with the theoretical value of 0.5 [21]. By extrapolating to $t = 0$, one can estimate the ground-state N atom density at the exit of the plasma. Plugging the $y$-intercepts of 0.605 and 0.354 into equation (1) (section 2) yields nitrogen atom densities of $9.9 \times 10^{15}\,\mathrm{cm}^{-3}$ and $2.9 \times 10^{16}\,\mathrm{cm}^{-3}$ for the $\alpha$ and $\gamma$ discharges, respectively. The power density in the $\alpha$ mode is $25\,\mathrm{W\,cm}^{-3}$, whereas in the $\gamma$ mode, it is $2083\,\mathrm{W\,cm}^{-3}$. Evidently, the much higher power absorption in the latter case does not translate into a much higher fraction of dissociated $N_2$ molecules. It should be pointed out that the N atom density estimated from the $N_2(B)$ decay profile is an average over the entire plasma volume. As can be seen in figure 7, the $\gamma$-mode plasma is not uniformly distributed across the gap.

## 4. Discussion

We have investigated the operation of an atmospheric pressure, RF plasma fed with helium and 0.4 vol% nitrogen. The transition from one operating regime to another is accompanied by a 40% reduction in voltage, and a surge in power density of 85 times. The $V$–$I$ phase angle changes from 88.9° to 45.7°, indicating that the plasma has become more resistive. The spatial emission profiles presented in figures 5 through 8 provide convincing evidence that the two operating regimes correspond to $\alpha$- and $\gamma$-mode discharges, with the principal ionization processes occurring in the bulk gas and at the electrode surfaces, respectively.

For the $\gamma$-mode plasma, a large temperature gradient most probably exists across the gap between the electrodes. Intense ion flux from the sheath to the electrodes will heat up the metal surfaces, while the flowing gas in the centre remains relatively cool. This temperature gradient may explain the barbell shape of the $\gamma$ discharge (cf figure 7). As the charged species move away from the boundaries, the gas cools and contracts into a much narrower and dimmer plasma column. This phenomenon may make it difficult to operate this discharge over large areas. For power densities ranging between 120 and $314\,\mathrm{W\,cm}^{-2}$, the diameter of the discharge at the electrode surfaces remained constant at about 4.5 mm. Note that when fluorine-containing gases are added to the helium, the negative ions stabilize the gamma discharge, and allow it to be operated over areas up to 25.0 mm in diameter [27].

The atmospheric pressure RF plasma may be modelled as a series connection of two capacitors and a resistor. Each of the capacitors represents one of the sheaths, while the resistor represents the bulk plasma [29]. The sheath capacitance may be calculated from the reactance measured by the impedance probe,

$$C = \frac{1}{2\pi f X}, \tag{2}$$

where $f$ is the frequency of the RF power (13.56 MHz) and $X$ is the reactance of the plasma (Ω). The total sheath thickness, $d_s$, can be calculated as

$$d_s = \frac{1.52\varepsilon_0 A}{C} = 1.52\varepsilon_0(2\pi f)XA. \tag{3}$$

Here, $\varepsilon_0$ is the permittivity of vacuum ($\mathrm{F\,m}^{-1}$), and $A$ is the discharge area ($\mathrm{m}^2$). In addition, the voltage drop across the sheath may be determined by

$$V = \frac{I}{2\pi f C}, \tag{4}$$

where $I$ is the total current.

From the quantities given above, the sheath thickness has been calculated right before and after the $\alpha$–$\gamma$ transition, i.e. points B and C in figure 3. It equals 25.7 $\mu$m (×2) in the $\alpha$ mode, for a reactance of 772 Ω and a discharge area of $7.6 \times 7.6\,\mathrm{mm}^2$. In contrast, the sheath thickness equals only 1.9 $\mu$m (×2) in the $\gamma$ mode given that the reactance is 449 Ω and the discharge has shrunk to 3 mm diameter discs on the electrodes. Thus, the sheath thickness decreases 13 times from the $\alpha$ to the $\gamma$ mode, indicating that its breakdown is responsible for the change in plasma operation [8, 29].

Knowing the sheath thickness and its voltage drop allows one to calculate the properties of the bulk plasma. The electron density, $n_e$, may be calculated from

$$J = -en_e\mu_e E, \tag{5}$$

where $J$ is the current density ($\mathrm{A\,m}^{-2}$), $e$ is a unit of charge (C), $\mu_e$ is the electron mobility ($\mathrm{V\,m}^{-1}\,\mathrm{s}^{-1}$) and $E$ is the bulk electric field ($\mathrm{V\,m}^{-1}$). The average electron temperature is calculated from a steady-state power balance on the free electrons in the plasma [44]. The electron density and temperature are estimated to be $5.7 \times 10^{12}\,\mathrm{cm}^{-3}$ and 1.0 eV in the $\alpha$ mode at point B on the $I$–$V$ curve. By comparison, the electron density and temperature are $1.8 \times 10^{13}\,\mathrm{cm}^{-3}$ and 1.5 eV in the $\gamma$ mode at point C on the $I$–$V$ curve.

Raizer *et al* [29, 30] have established that in moderate-pressure RF plasmas, the $\alpha$–$\gamma$ transition occurs if the plasma density exceeds a critical value for sheath breakdown. It is of interest to calculate this value, and compare it to the maximum electron density obtained in the $\alpha$ mode. The $\alpha$–$\gamma$ transition occurs when the oscillation amplitude of the plasma boundary ($A'$) exceeds the total sheath thickness, i.e. $2A' = d_s$. The critical electron density is given by [29, 30]:

$$n_{\mathrm{critical}} = \frac{Bp}{(e/\varepsilon_0)A'[\ln(A/\ln(1+\gamma^{-1})) + \ln(2pA')]}, \tag{6}$$

where $A$ and $B$ are constants for helium gas (2.8 and 34 V cm$^{-1}$ Torr$^{-1}$), $p$ is the pressure (Torr) and $\gamma$ is the secondary electron emission coefficient of the electrodes (0.01 for aluminium). The error introduced by using constants for He gas should be negligible, since only 0.4 vol% nitrogen was added to the discharge. Assuming $A' = d_s/2 = 25.7\ \mu$m right before the transition, one obtains critical plasma and current densities of $6.4 \times 10^{12}$ cm$^{-3}$ and 0.76 A cm$^{-2}$. These values agree well with the electron and current densities determined at point B on the $I$–$V$ curve: $5.7 \times 10^{12}$ cm$^{-3}$ and 0.71 A cm$^{-2}$, respectively.

We have shown that the $\alpha$-mode helium and nitrogen plasma generates a maximum N atom concentration of $9.9 \times 10^{15}$ cm$^{-3}$ at a power density of 25 W cm$^{-3}$. This corresponds to 5.2% dissociation of the $N_2$ molecules. In contrast, the $\gamma$-mode helium and nitrogen plasma produces a maximum concentration of N atoms of $2.9 \times 10^{16}$ cm$^{-3}$ at a power density of 2083 W cm$^{-3}$. This N atom density is equivalent to 15.2% dissociation of the $N_2$ molecules. These results indicate that the abnormal glow is nearly as effective as the $\gamma$ mode, which consumes 85 times more power. However, examination of the picture of the latter discharge in figure 7 reveals that only about one-sixth of the area between the electrodes is illuminated by the plasma. This suggests that within the active glow discharge, $N_2$ dissociation could be close to 100%.

## 5. Conclusions

We have investigated the properties of the $\alpha$ and $\gamma$ operating modes of an atmospheric pressure, RF, helium and nitrogen plasma. It has been shown that beyond critical plasma and current densities of $5.7 \times 10^{12}$ cm$^{-3}$ and 0.71 A cm$^{-2}$, sheath breakdown occurs so that the primary ionization pathway shifts from the bulk gas to the electrode surfaces. With 0.4 vol% $N_2$ in the system, the $\alpha$- and $\gamma$-mode discharges produce $9.9 \times 10^{15}$ cm$^{-3}$ and $2.9 \times 10^{16}$ cm$^{-3}$ N atoms, respectively.

## Acknowledgments

This work was supported by a University of California Discovery grant and by a contract with Surfx Technologies LLC.

## References

[1] Roth J R 1995 *Industrial Plasma Engineering* vol I *Principles* (Philadelphia, PA: Institute of Physics Publishing)
[2] Lieberman M A and Lichtenberg A J 1994 *Principles of Plasma Discharges and Materials Processing* (New York: Wiley)
[3] Schütze A, Jeong J Y, Babayan S E, Park J, Selwyn G S and Hicks R F 1998 *IEEE Trans. Plasma Sci.* **26** 1685
[4] Fauchais P and Vardelle A 1997 *IEEE Trans. Plasma Sci.* **25** 1258
[5] Alexeff I and Laroussi M 2002 *IEEE Trans. Plasma Sci.* **30** 174
[6] Yu L, Laux C O, Packan D M and Kruger C H 2002 *J. Appl. Phys.* **91** 2678
[7] Storch D G and Kushner M J 1993 *J. Appl. Phys.* **73** 51
[8] Shi J J, Deng X T, Hall R, Punnett J D and Kong M G 2003 *J. Appl. Phys.* **94** 6303
[9] Yuan X and Raja L L 2003 *IEEE Trans. Plasma Sci.* **31** 495
[10] Chang J S, Lawless P A and Yamamoto T 1991 *IEEE Trans. Plasma Sci.* **19** 1152
[11] Massines F, Segur P, Gherardi N, Khamphan C and Ricard A 2003 *Surf. Coat. Technol.* **174–175** 8
[12] Kunhardt E E 2000 *IEEE Trans. Plasma Sci.* **28** 189
[13] Schoenback K H, Verhappen R, Tessnow T, Peterkin F E and Byszewski W W 1996 *Appl. Phys. Lett.* **68** 13
[14] Roth J R, Sherman D M, Gadri R B, Karakaya F, Chen Z, Montie T C, Kelly-Wintenberg K and Tsai P Y 2000 *IEEE Trans. Plasma Sci.* **28** 56
[15] Moisan M, Zakrzewski Z, Etemadi R and Rostaing J C 1998 *J. Appl. Phys.* **83** 5691
[16] Jeong J Y, Babayan S E, Tu V J, Henins I, Velarde J, Selwyn G S and Hicks R F 1998 *Plasma Sources Sci. Technol.* **7** 282
[17] Jeong J Y, Park J Y, Henins I, Babayan S E, Tu V J, Selwyn G S, Ding G and Hicks R F 2000 *J. Phys. Chem.* **104** 8027
[18] Tu V J, Jeong J Y, Schütze A, Babayan S E, Selwyn G S, Ding G and Hicks R F 2000 *J. Vac. Sci. Technol.* A **18** 2799
[19] Park J, Henins I, Hermann H W, Selwyn G S and Hicks R F 2001 *J. Appl. Phys.* **89** 20
[20] Babayan S E, Jeong J Y, Schütze A, Tu V J, Moravej M, Selwyn G S and Hicks R F 2001 *Plasma Sources Sci. Technol.* **10** 573
[21] Babayan S E, Ding G and Hicks R F 2001 *Plasma Chem. Plasma Process.* **21** 505
[22] Nowling G R, Babayan S E, Jankovic V and Hicks R F 2002 *Plasma Sources Sci. Technol.* **11** 97
[23] Babayan S E, Ding G, Nowling G R, Yang X and Hicks R F 2002 *Plasma Chem. Plasma Process.* **22** 255
[24] Yang X, Babayan S E and Hicks R F 2003 *Plasma Sources Sci. Technol.* **12** 484
[25] Moravej M, Babayan S E, Nowling G R, Yang X and Hicks R F 2004 *Plasma Sources Sci. Technol.* **13** 8
[26] Yang X, Moravej M, Babayan S E, Nowling G R and Hicks R F 2004 *J. Nucl. Mater.* **324** 134
[27] Yang X, Moravej M, Babayan S E, Nowling G R and Hicks R F 2005 *Plasma Sources Sci. Technol.* submitted
[28] Levitskii S M 1957 *Sov. Phys.—Tech. Phys.* **2** 887
[29] Raizer Y P, Shneider M N and Yatsenko N A 1995 *Radio-Frequency Capacitive Discharge* (Boca Raton, FL: CRC Press)
[30] Raizer Y P and Shneider M N 1987 *Sov. J. Plasma Phys.* **13** 267
[31] Raizer Y P and Shneider M N 1991 *Sov. J. Plasma Phys.* **17** 789
[32] Raizer Y P and Shneider M N 1992 *Sov. J. Plasma Phys.* **18** 762
[33] Godyak V A, Piejak R B and Alexandrovich B M 1991 *IEEE Trans. Plasma Sci.* **19** 660
[34] Simek M and De Benedictis S 1995 *Plasma Chem. Plasma Process.* **15** 451
[35] Noxon J F 1962 *J. Chem. Phys.* **36** 926
[36] Young R A and Black G 1965 *J. Chem. Phys.* **44** 3741
[37] Campbell I M and Thrush B A 1967 *Proc. R. Soc.* A **296** 201
[38] Stoffels E, Flikweert A J, Stoffels W W and Kroesen G M W 2002 *Plasma Sources Sci. Technol.* **11** 383
[39] Guo Y B and Hong F C N 2003 *Appl. Phys. Lett.* **83** 337
[40] Pearse R W B and Gaydon A G 1976 *The Identification of Molecular Spectra* (London: Chapman and Hall)
[41] Reader J and Corliss C H 1980 *Wavelengths and Transition Probabilities for Atoms and Atomic Ions* (Washington, DC: US Government Printing Office)
[42] Filippelli A R, Sharpton F A and Lin C L 1982 *J. Chem. Phys.* **76** 3597
[43] Umemoto H, Terada N, Tanaka K and Oguro S 2000 *Phys. Chem. Chem. Phys.* **2** 3425
[44] Mitchner M and Kruger C H 1973 *Partially Ionized Gases* (New York: Wiley)